ACS APPLIED MATERIALS & INTERFACES

Research Article

www.acsami.org

Bioinspired Zwitterionic Surface Coatings with Robust Photostability and Fouling Resistance

Chun-Jen Huang,*[,†,#] Sz-Hau Chu,[†] Lin-Chuan Wang,[†] Chien-Hung Li,[‡] and T. Randall Lee[‡]

[†]Department of Biomedical Sciences and Engineering and [#]Department of Chemical and Materials Engineering, National Central University, Jhong-Li, Taoyuan 320 Taiwan

[‡]Department of Chemistry and the Texas Center for Superconductivity, University of Houston, Houston, Texas 77204-5003 United States

Supporting Information

ABSTRACT: Great care has been paid to the biointerface between a bulk material and the biological environment, which plays a key role in the optimized performance of medical devices. In this work, we report a new superhydrophilic adsorbate, called L-cysteine betaine (Cys-b), having branched zwitterionic groups that give rise to surfaces and nanoparticles with enhanced chemical stability, biofouling resistance, and inertness to environmental changes. Cys-b was synthesized from the amphoteric sulfur-containing amino acid, L-cysteine (Cys), by quaternization of its amino group. Gold surfaces modified with Cys-b exhibited prominent repellence against the nonspecific adsorption of proteins, bacteria, and fibroblast cells. In addition, Cys-b existed in zwitterionic form over a wide pH range (i.e., pH 3.4 to 10.8), and showed excellent suppression in photoinduced oxidation on gold substrates. Furthermore, the modification of hollow Ag@Au nanoshells with Cys-b gave rise to nanoparticles with excellent colloidal stability and resistance to coordinative interaction with Cu^{2+}. Taken together, the unique features of Cys-b offer a new nanoscale coating for use in a wide spectrum of applications.

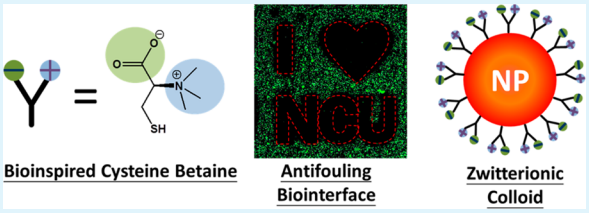

KEYWORDS: *zwitterionic materials, antifouling coatings, nanomaterials, biocompatible, bioinspired materials*

INTRODUCTION

Advances in nanobiotechnology and the corresponding nanomaterials offer substantial impacts on therapeutic and diagnostic applications. The unique physicochemical characteristics of nanomaterials are particularly important, with plasmonic gold nanoparticles (AuNPs) and fluorescent quantum dots (QDs) attracting considerable attention. Until now, the scope of materials has expanded to include silicon dots, carbon dots, alloyed plasmonic nanoparticles, and gold nanoclusters.[1,2] The development of nanoparticles has reached a high level, and the size, shape, and surface characteristics of NPs have been intensively studied, giving rise to a tremendous impact on their biocompatibility, biodistribution, and unique functions.[3,4] However, implementation of these nanoparticles in unfiltered and unpurified bodily fluids such as blood, urine, or saliva is still challenging owing to the formation of a dynamic biomolecular corona.[4] Occurrence of the biomolecular corona involves the nonspecific adsorption of proteins, lipids, and other biomolecules, leading to unpredictable and uncontrollable behaviors of NPs to achieve their exploitation in nanomedicine. Therefore, great care must be paid to the interface between a nanoparticle core and the biological environment, which is a key area to be engineered carefully for optimized performance.

Enormous efforts have been devoted to developing toolkits for engineering surfaces with an attempt to meet desirable interfacial properties, such as wettability, surface charges, free energy, and chemical functionality.[5−7] Over two decades, attention has focused on self-assembled monolayers (SAMs) because of their unique properties, such as control on the molecular level, ordered structure, high packing density, ease of preparation, and functionalization.[8] Importantly, self-assembling capping ligands (i.e., molecular adsorbates) provide a facile coating approach to modify surfaces to achieve specific applications.[8−10] To achieve biocompatibility in NP systems, the predominant focus has been on the attachment of thiolated polyethylene glycol (PEG) adsorbates, usually with large molecule weights.[11−13] Besides an increase in hydrodynamic diameter, critical issues with PEG materials are the ease of oxidation in the presence of oxygen and transition metal ions,[14−16] and their susceptibility to hydration as a function of temperature and ionic strength.[17−19]

Inspired by the zwitterionic structures in polar phospholipids, the Whitesides group carried out pioneering tests with zwitterionic SAMs on gold substrates, showing their biofouling resistance and environmental stability.[20] Two ionic SAM systems were accomplished: mixed and single-component SAMs. The mixed SAMs were formed from a 1:1 combination of positively and negatively charged thiols. On the other hand, the single-component SAMs were prepared from thiols

Received: September 8, 2015
Accepted: October 9, 2015
Published: October 9, 2015

DOI: 10.1021/acsami.5b08418
ACS Appl. Mater. Interfaces 2015, 7, 23776−23786

Scheme 1. Molecular Structures and Formation of SAMs from L-Cysteine (Cys) and L-Cysteine Betaine (Cys-b) on Gold Substrates under Physiological Conditions

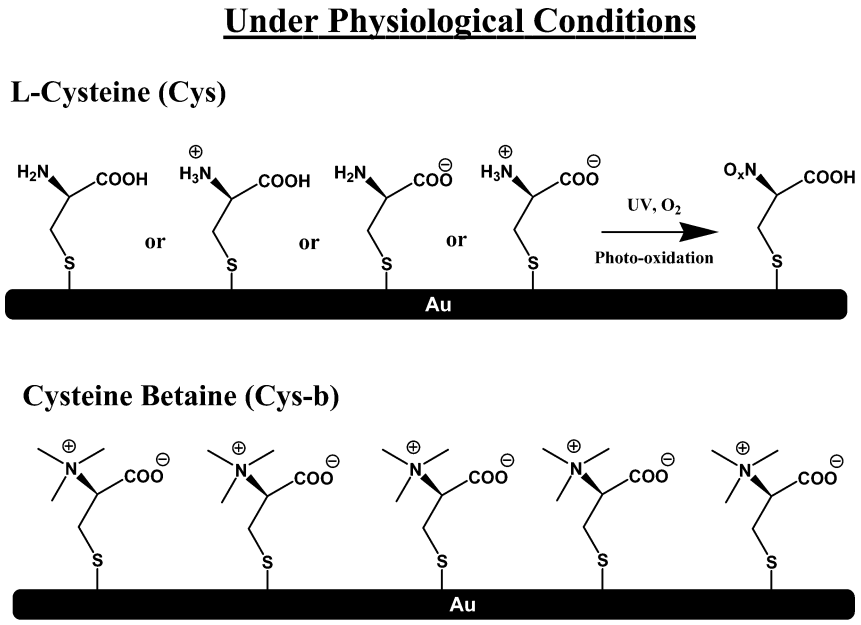

terminating in groups combining both a cationic moiety and an anionic moiety. The charged groups included ammonium, sulfonate, and phosphoric acid. The effectiveness of zwitterionic materials relies on their strong hydration and charge balance, leading to a thermodynamic reduction in the entropy gain and the enthalpy loss against protein adsorption. In recent years, several zwitterionic materials have been successfully developed with different structural diversity of ionic polar groups, including sulfobetaine (SB), phosphorylcholine (PC), and carboxybetaine (CB).[7,21−23]

Several natural zwitterionic organosulfur compounds have been used for the modification of NPs and for improving their aqueous stability and biocompatibility. Bawendi et al. conducted the synthesis of L-cysteine (Cys)-coated quantum dots, showing a reduction in protein adsorption and enhanced biodistribution.[24] The Nienhaus group studied SAMs derived from D-penicillamine, which conferred enhanced chemical stability by inhibiting oxidation of the thiol-Au bond.[25,26] Although the zwitterionic Cys and D-penicillamine with branched ionic groups have found success as biocompatible NP coatings, their zwitterionic nature exists over a limited pH range, and the primary amine group on gold can be photo-oxidized to become nitrogen oxide, particularly upon exposure to UV irradiation.[27−29] Furthermore, according to previous reports, the coordination of Cys with Cu^{2+} forms a Cys-Cu^{2+}-Cys complex through displacement of the hydrogen bond between Cys by the coordination with Cu^{2+}.[30−32] Because of this highly specific coordination, several studies used this interaction to detect Cu^{2+} through the induced aggregation of Cys-modified nanoparticles, which leads to a shift in the extinction maximum or strong scattering.[32,33] Although progress in the detection of Cu^{2+} with Cys has been achieved, the studies also imply the restriction of Cys-capped nanoparticles for other purposes in the presence of Cu^{2+}.

In this study, we synthesized and characterized a new L-cysteine-derived zwitterionic molecule, called L-cysteine betaine (Cys-b), and explored its chemical robustness, environmental stability, and antifouling properties as a surface-modifying agent (Scheme 1). The molecular protonation behaviors of Cys and Cys-b as a function of pH were monitored by titration tests. The cytotoxicity of Cys-b was examined by MTT assay with NIH 3T3 fibroblasts. The corresponding SAMs prepared on gold substrates were characterized using contact angle goniometry and X-ray photoelectron spectroscopy (XPS) for the resulting wettability and elemental compositions, respectively. The antiphotooxidation and antifouling properties of Cys-b in comparison with Cys were unveiled by the XPS measurements, and protein, cell and bacterial adsorption studies. In addition, Cys-b and Cys were utilized to modify plasmonic hollow Ag@Au nanoshells to evaluate the effectiveness of the coatings with regard to colloidal stability and susceptibility to Cu^{2+}. This work not only opens up potential applications of novel bioinspired zwitterionic organosulfur ligand as a new nanoscale coating material, but also establishes molecular insight into the design of robust biocompatible interfaces.

EXPERIMENTAL SECTION

Materials. L-Cysteine (Cys), potassium hydroxide (KOH), dimethyl sulfate, trifluoroacetic acid (TFA), glacial acetic acid, acetone, silver nitrate, and potassium carbonate were purchased from Sigma-Aldrich. Trisodium citrate dihydrate and nitric acid were obtained from EM Science. Hydrogen tetrachloroaurate(III) hydrate ($HAuCl_4 \cdot H_2O$) was from Strem. Chicken hen egg white lysozyme, 3,3′,5,5′-tetramethylbenzidine (TMB), bovine serum albumin (BSA), and TWEEN 20 were obtained from MDBio Inc. Mouse-antimucin IgG, rabbit-anti-BSA IgG, horseradish peroxidase (HRP)-conjugated goat-antimouse IgG, and HRP-conjugated goat-antirabbit IgG were obtained from Thermo Scientific. Rabbit-antilysozyme IgG was acquired from LSBio. Dulbecco's Modified Eagle's Medium (DMEM) and fetal bovine serum (FBS) were from Gibco. Luria−Bertani broth (LB broth) was obtained from BD. Water was purified to a resistivity of 18 MΩ cm using the Academic Milli-Q Water System (Millipore Corporation) and filtered using a 0.22 μm filter. All glassware used in the experiments were cleaned in an aqua regia solution (3:1 HCl:HNO_3) and dried in an oven prior to use.

Synthesis of Cys-b. A flask containing 1 g of Cys in 3 mL of deionized water was immersed in an ice bath and stirred under

DOI: 10.1021/acsami.5b08418
ACS Appl. Mater. Interfaces 2015, 7, 23776−23786

nitrogen. Two additional funnels were set up, one with 8.5 mL of 6.5 M KOH and another with 5.2 mL of dimethyl sulfate. KOH was introduced dropwise until dissolving the Cys. The residual KOH and dimethyl sulfate were dropped in simultaneously for 1 h with stirring. Afterward, the flask was kept for another 20 min at room temperature (rt), and then 1.2 mL of glacial acetic acid was added. The reaction solution was evaporated in vacuo to a volume of around 2 mL. Byproduct potassium methyl sulfate was precipitated by adding 40 mL of ethanol and then filtered using filter paper. The filtrate was concentrated using a rotovap to a volume of around 2 mL, and then precipitated by adding 50 mL of acetone. The white product was washed with acetone 5 times to afford pure cystine betaine. Cystine betaine was reduced in 0.1 M dithiothreitol (DTT) in deionized water and stirred at 65 °C for 2 h. After cooling, 50 mL of acetone was added to precipitate the white product of Cys-b. The product was collected and dried (70% yield). The scheme for the synthesis of Cys-b and its ^{1}H NMR spectrum are shown in Figure S1.

Potentiometric Titrations. Potentiometric titrations of aqueous solutions were conducted using a pH meter (Clean Instrument, PH500, US) glass electrode. Cys and Cys-b solutions were prepared at 0.1 M in deionized water, and the pH of the solutions was adjusted to pH 1 by adding 0.1 M HCl. The pH values were recorded while dropping 0.1 N NaOH until pH 13. The acid dissociation constant (pK_a) and isoelectric point (pI) were then determined by plotting the titration curves for Cys and Cys-b.

Cytotoxicity Tests. NIH 3T3 fibroblasts were cultured in a 24-well plate with a seeding concentration of 1×10^4 cell/mL in DMEM containing 10% of FBS at 37 °C in a 5% CO_2 incubator. After incubation for 16 h, the medium was replaced by serum-free DMEM containing Cys or Cys-b at different concentrations for an additional 24 h culturing. MTT assay was performed for assessing cell metabolic activity. The MTT solution was added to the culture medium to a final concentration of 0.5 mg/mL. After incubation for 3 h, the medium was replaced by DMSO, and the absorbance of the solution was quantified by UV−vis spectroscopy at 540 nm (V-630, JASCO, MD). The reported values are the mean from three replicates and are expressed as percentages with respect to the control values.

Formation of SAMs. A gold substrate was prepared by deposition onto a 20 mm × 20 mm glass slide in a high-vacuum e-beam evaporator. A 5 nm thick chromium layer was first deposited as an adhesive layer before the addition of a 50 nm thick layer of high purity gold. The Au substrates were cleaned sequentially in a sonication bath of 0.1% SDS, acetone, and ethanol for 10 min each, followed by drying in a stream of nitrogen. The substrates were transferred to a plasma cleaner (PDC-001, Harrick Plasma, NY) to expose O_2 plasma twice with a power of 10.5 W for 10 min to remove trace amounts of contaminants from the surfaces. The clean substrates were immediately immersed into a 1 mM Cys or Cys-b solution in deionized water containing 2% TFA and shaken at 50 rpm at rt for 12 h. The modified substrates were removed and cleaned with deionized water, ethanol containing 5% ammonium hydroxide, and water, followed by drying in a stream of nitrogen.[34]

Contact Angle Measurements. Static water contact angles were accessed by using an optical contact angle goniometer (Phoenix mini, Surface Electro Optics, Seoul). The 5 μL water droplets from a microsyringe were placed on the substrates, and the contact angles were measured at least three times at random positions.

XPS Measurements. The elemental spectra were collected by XPS with a microfocused and monochromatic Al Kα X-ray source (1486.6 eV, 400 μm; Sigma Probe, Thermo Scientific). The takeoff angle (with respect to the surface) of the photoelectron was set at 45°. The pressure of the system was below 10^{-10} Pa using an oil-less ultrahigh vacuum pumping system. A dual beam charge neutralizer (7 V Ar^+ and flooding 3 kV, 1 μA electron beam) was employed to compensate for charging effects. Spectra were collected with a pass energy set to 58.7 eV, while the binding energy measured was calibrated against the Au 4f peaks at 84 and 88 eV. The typical data acquisition time was around 30 min.

Bacterial Fouling Tests. A single bacteria colony of *S. epidermidis* or *P. aeruginosa* was picked from the LB agar plate to inoculate 25 mL liquid LB growth media. After 16 h inoculation at 37 °C shaking at 200 rpm, 1 μL bacteria containing media from the first culture was used for a secondary culture also in LB in a conical flask. The bacteria were then washed with sterile PBS solution three times through centrifugation at 4000 rpm for 5 min and resuspension in PBS. After the final wash, the bacterial samples in PBS were diluted to an optical density reading at 670 nm (OD670) of 0.1, corresponding to $\sim 8 \times 10^7$ cells/mL, to be tested for antifouling properties of substrates. The substrates were dipped into the bacterial solution at 37 °C for 3 h, followed by washing with sterile PBS and shaking at 100 rpm for 5 min for three times. The adsorbed bacteria were stained with 50 μL of LIVE/DEAD BacLight and covered with paraffin for 15 min. Afterward, the substrates were observed under fluorescence microscopy (ZEISS Microscope Axio Obserber A1, Germany) with a magnification of 400× and an excitation wavelength of 488 nm. The measurements were performed at five random locations on each sample, and the bacteria numbers were analyzed using an ImageJ software package (developed at National Institutes of Health, MA).

Enzyme-Linked Immunosorbent Assay (ELISA) for Protein Fouling Tests. BSA, lysozyme, and mucin were dissolved in PBS at a concentration of 4.9 mg/mL for BSA, 2.0 mg/mL for lysozyme, and 0.25 mg/mL for mucin. The substrates were transferred to a 6-well plate that contained 4 mL of protein solution in each well at rt for 3 h. After removal from the protein solutions, the substrates were washed with PBST (PBS containing 0.05 wt % of TWEEN 20) for 5 min at 120 rpm for 3 times. The substrates were separately immersed in solutions containing rabbit anti-BSA IgG, rabbit antichicken-egg lysozyme IgG, and mouse antimucin IgG with 1:5000 dilution for 1 h at rt. After removal from the primary-antibody solutions, the substrates were then washed with PBST for 5 min at 120 rpm for 3 times. The substrates were subsequently incubated with corresponding HRP-conjugated secondary antibodies with 1:5000 dilution for 1 h at rt. After washing with PBST for 5 min at 120 rpm for 3 times, the substrates were brought to contact with TMB for 10 min and stop reaction with 1 M H_2SO_4 (molar ratio of TMB:H_2SO_4 = 2:1). The supernatants were read at OD 450 nm to estimate the relative protein fouling level.

Cell Adhesion Tests. The substrates were sterilized in 75% ethanol for 30 s and then washed with PBS for 3 min before cell seeding. The substrates were placed in a 24-well plate, and 3T3 fibroblasts in DMEM with 1% FBS were introduced with a total cell number of 2×10^5 per well. After culturing for 72 h, the substrates were removed and washed with PBS, followed by imaging under an optical microscope. The cell number and cell coverage area were estimated using ImageJ software.

Preparation of Gold−Silver Nanoshells. Silver nanoparticles were prepared by the method of Lee and Meisel,[35] which involves the reduction of $AgNO_3$ by sodium citrate. An aliquot of $AgNO_3$ (0.0340 g, 0.200 mmol) was dissolved in 200 mL of H_2O. The solution was brought to reflux, and then 4 mL of 1% trisodium citrate solution was added under vigorous stirring. The solution continued to reflux for 25 min. The contents turned a yellow green color, indicating the presence of silver nanoparticles. The solution was allowed to cool to rt and then centrifuged at 6000 rpm for 15 min. The nanoparticles were then redispersed in 25 mL of water. This procedure generated monodispersed silver nanoparticles, where the size could be adjusted from 40 to 100 nm, depending on the concentration of the reactants. For the synthesis of hollow gold−silver nanoshells, we followed the procedure reported in our previous papers.[36,37] The basic solution of gold salt (K-gold solution) was prepared using the method reported by Oldenburg et al.[38] In this method, 0.050 g of K_2CO_3 was added to 200 mL of purified water, which was then injected into 4 mL of 1% $HAuCl_4 \cdot H_2O$ solution. The mixture, initially yellow in color, became colorless 30 min after the reaction was initiated. The flask was then covered with aluminum foil to shield it from light, and the solution was stored in a refrigerator overnight. To obtain a surface plasmon resonance (SPR) band at ~800 nm using the gold−silver nanoshell solutions, 20 mL of silver nanoparticles solution mixed with 200 mL K-gold solution and stirred for 4 h. The SPR band of the solution was tracked using UV−vis measurements. The nanoshells were isolated by

DOI: 10.1021/acsami.5b08418
ACS Appl. Mater. Interfaces 2015, 7, 23776−23786

centrifugation at 6000 rpm for 15 min, and the supernatant was then decanted. The particles were redispersed in 22.5 mL of water. The size and morphology of the nanoparticles were evaluated using a LEO-1525 scanning electron microscope (SEM, Carl Zeiss, Germany) operating at an accelerating voltage of 15 kV, and dynamic light scattering (DLS, Nano-S, Malvern, UK). Extinction spectra were obtained using a UV−vis spectrometer obtained over the wavelength range of 200 to 1000 nm with all the nanoshell samples suspended in PBS for the measurements.

Colloidal Stability Tests. For the nanoparticle modification, the total amount of the ligands Cys and Cys-b was 1×10^7, equivalent to nanoparticles in deionized water. The modification proceeded for 12 h at rt, followed by collecting and washing with PBS via centrifugation at 9000 rpm for 10 min. The particles were resuspended in PBS. The changes in SPR maxima and particle sizes were accessed using UV−vis spectroscopy and DLS. With regard to the effect of multivalent ions on the colloidal stability, 1 mM of Cu^{2+} solution was prepared from CuCl and mixed with modified nanoparticles for 1 h at rt. The colloidal stability of nanoparticles with and without the modification of Cys or Cys-b in the presence of Cu^{2+} ions was followed using UV−vis spectroscopy.

RESULTS AND DISCUSSION

Synthesis and Characterization of Cys-b. The Cys-b molecules were successfully synthesized through quaternization of the amino group of cystine, followed by the reduction of the disulfide bond.[39] The product was crystallized and dried under vacuum. The chemical structure of Cys-b was verified using ^{1}H NMR spectroscopy as shown in the Supporting Information (Figure S1b), and the mass-to-charge ratio (m/z) of 165.15 was confirmed by electrospray ionization mass spectrometry.

The amphoteric amino acids contain both acidic and basic groups, and thus their predominant form depends on the pH of the solution. The acid−base properties of Cys and Cys-b were monitored by dissolving the molecules in deionized water and titrating from pH 1 to pH 13 as shown in Figure 1. The pK_a

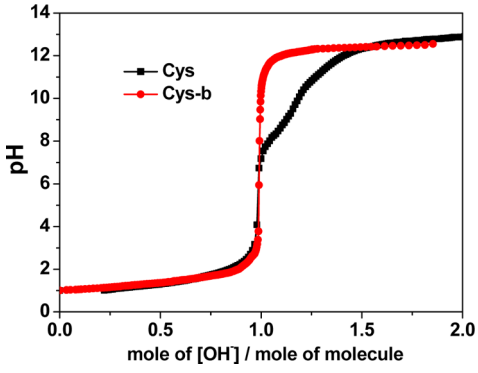

Figure 1. Potentiometric titration curves of Cys and Cys-b at a concentration of 0.1 M in deionized water.

values for the −COOH and protonated $-NH_2$ groups on the α-carbon, and the −SH group on the side chain of Cys are 1.5, 10.7, and 8.5, respectively, which are consistent with the reported values in the literature.[40] The isoelectric point (pI) of Cys was estimated as 5.0. Additionally, the zwitterionic form of Cys existed over the pH range from 3.2 to 7.2. For Cys-b, the feature of the titration curve is significantly different from that of Cys because of the presence of the quaternary ammonium cation that is permanently positively charged and independent of the pH. We can only find the pK_a values of the −COOH group and the −SH group of Cys-b, which are 1.6 and 12.6, respectively. The pI value of Cys-b is 4.4. The zwitterionic character of Cys-b exists over a wide pH range from 3.4 to 10.8. In addition, the neutral form of Cys-b over the wide pH range reflects the fact that the cationic ammonium serves as an electron-withdrawing substituent, facilitating the deprotonation of the carboxyl group, which confers tolerance of molecular polarity toward the pH changes. In other words, Cys-b can endure pH fluctuation and still ensure charge balance under various conditions.

The cytotoxicity of natural Cys and synthetic Cys-b was accessed by dissolving in serum-free culture medium at concentrations from 5 μM to 5 mM and incubating with NIH 3T3 fibroblasts for 16 h. The MTT assay was applied to monitor the cell viability as shown in Figure 2. The data

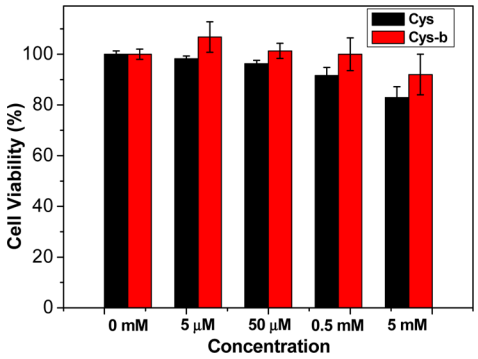

Figure 2. Cytotoxicity of Cys and Cys-b at concentrations from 5 μM to 5 mM in serum-free culture medium. The amino acids incubated with NIH 3T3 fibroblasts cells for 16 h prior to MTT assay.

indicated that the cell viability of Cys-b remained above 90% at a concentration up to 5 mM, which was slightly higher than Cys. Therefore, the results indicated that the negligible cytotoxicity of Cys-b offers potential uses as a nanoscale coating material for implants and other medical devices.

Cys-b SAM Formation. It has been suggested that Cys SAMs might form a double layer through the formation of hydrogen bonds[41,42] and/or ion pairing between oppositely charged groups on the terminal groups of bound thiolate on the surface and free thiols in the bulk.[43] The coating solutions were prepared by adding a small amount of TFA to eliminate the charge interaction, followed by washing the substrates with an ethanolic solution of ammonium hydroxide to remove hydrogen bonds. Compared with the coatings prepared from only the aqueous solution, the Cys and Cys-b films with acid and base treatments exhibit better hydrophilicity, which is indicated by the small contact angles of 8.0 ± 0.9° and 7.0 ± 1.2°, respectively (Figure 3 and Figure S2). Herein, the difference in the contact angles for Cys and Cys-b substrates is insignificant. According to the quantitative analysis with high-resolution spectroscopy by Rolandi et al., the ratio of zwitterionic to neutral forms of adsorbed Cys on Au is 3:1.[44] The work supported the observation of the superhydrophilic property of the Cys film in which the strong interaction with water molecules was induced through ionic solvation and hydrogen bonding.[45−48] For Cys-b films, the robust zwitterionic structure ensures the good wettability.

In addition, the XPS spectra revealed the elemental compositions of the Cys and Cys-b coatings; the atomic concentrations of C, N, O, and S are given in Table S1. The measured ratios of N/S on Cys and Cys-b films were 0.95 and 1.07, respectively, which are comparable to the estimated

DOI: 10.1021/acsami.5b08418
ACS Appl. Mater. Interfaces 2015, 7, 23776−23786

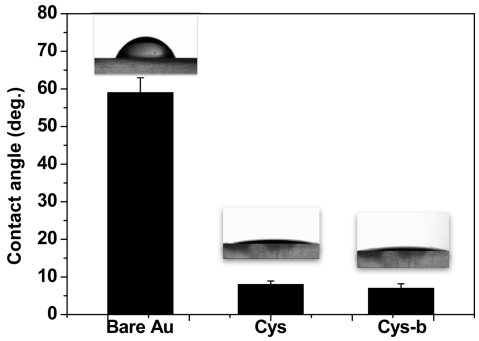

Figure 3. Contact angle measurements for bare Au and Au coated with Cys and Cys-b. The modified substrates were prepared using an optimized procedure to avoid the formation of double layers.

values. Therefore, the formation of Cys and Cys-b films on Au can be confirmed for the physicochemical studies and application in fouling resistance from the contact angle and XPS measurements.

Suppression of Photoinduced Oxidation with Cys-b SAMs. We were intrigued and inspired by a previous study in which Shyue et al. reported that amino-terminated SAMs on Au surfaces can be oxidized under exposure to light and oxygen.[28] Herein, we investigated the effect of photoinduced oxidation on the chemical stability of Cys and Cys-b SAMs by contact angle and XPS measurements. The modified substrates were placed in the presence or absence of ambient air and light. The other experimental conditions were to store samples in darkness by covering an aluminum foil or in air-free ethanol, which were tested to control the exposure to light and oxygen.[28] After 8 h aging, the samples were removed, and their wettability by water was measured (Figure 4). The results revealed that the Cys and Cys-b SAMs in the absence of air and light retained their hydrophilicity. However, the contact angles of water on the Cys SAMs increased to 29 ± 1.5°, 28 ± 0.7°, and 60 ± 3.2° upon exposure to air, light, and both conditions, respectively. On the contrary, the wettability of the Cys-b SAMs (θ < 13°) was largely independent of the experimental conditions.

In addition, we conducted measurements to follow the changes in the contact angles of water on the Cys and Cys-b SAMs upon exposure to UV irradiation (at λ = 365 nm and a dose of 1.6 mW/cm^2) in the ambient environment (with 21% oxygen by volume). As illustrated in Figure 4b, the increases in the contact angles on the Cys SAMs is significantly higher than that on Cys-b SAMs. The contact angles on both samples reached a plateau after 8 h of continuous irradiation.

The aging tests showed that the wettability of the Cys SAMs deteriorated over time, leading the interfacial chemical environment to be less polar. In contrast, the Cys-b SAMs, with three methyl substituents on the amino group, exhibited exceptional resistance against the aging process. In previous work involving amine-terminated SAMs on gold, the amino group, when subjected oxidation by exposure to air and light, was converted into a nitroso group.[28] The change proceeded likely via a photoactive reaction. If the Cys SAMs react analogously, quaternization of the amine can effectively eliminate the photooxidation due to the occupation of all free electrons of the amine by the nucleophilic substitution. However, one might suspect that the decrease in hydrophilicity can be due to oxidation of the thiolates, leading to the desorption of the SAMs.[49−52] To address this concern, we further investigated the elemental compositions of the SAMs upon aging using XPS.

XPS was used to determine the chemical state of the N and S atoms of the Cys and Cys-b SAMs upon aging in the presence of the light and oxygen. Figure 5 displays the XPS spectra of as-prepared and aged samples. In the N 1s spectra for the as-prepared SAMs, we assign the peaks at binding energy (BE) = 399.9, 401.7, and 403.1 eV to $-NH_2$, $-NH_3^+$, and $-N(CH_3)_3^+$, respectively (Figures 5a and 5b).[53] From the XPS analysis, the protonation ratio of the amine groups on the as-prepared Cys SAMs was about 77%, which gives rise to high polarity and confirms its high wettability in the contact angle measurements, and is further consistent with previous work.[44] After the aging tests, the intensity of the peak for $-NH_3^+$ decreases significantly, and a new peak appears at BE = 401.2 eV, which we attribute to the oxidation of nitrogen (−NO).[28] Moreover, the O 1s spectrum for the aged Cys SAM confirmed the photoinduced oxidation of nitrogen by the appearance of a new peak at 532.9 eV, assigned to the nitroso group (Figure 5c).[54] The change in the XPS spectra reveals the oxidation of the primary amine groups of the Cys coatings in the aging test. In contrast, we observe no corresponding evidence for the oxidation of nitrogen on the Cys-b SAMs, demonstrating its chemical stability against the photoinduced oxidation.

Regarding the possible oxidation of the thiolate groups during the aging tests, we monitored the chemical state of

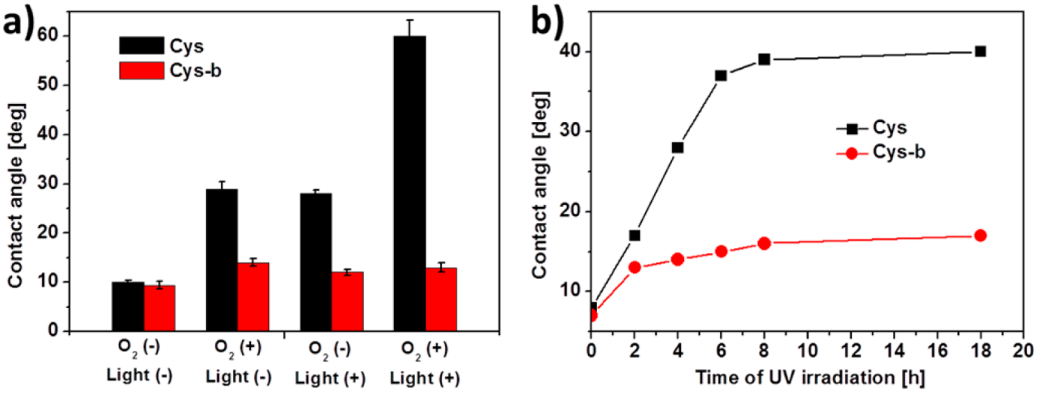

Figure 4. Contact angles of water for the assessment of photoinduced oxidation on Cys and Cys-b SAMs. (a) The samples were aged in the presence (denoted by "+") or absence (denoted by "-") of ambient air and light. (b) The contact angles of water on Cys and Cys-b SAMs as a function of UV exposure time.

DOI: 10.1021/acsami.5b08418
ACS Appl. Mater. Interfaces 2015, 7, 23776−23786

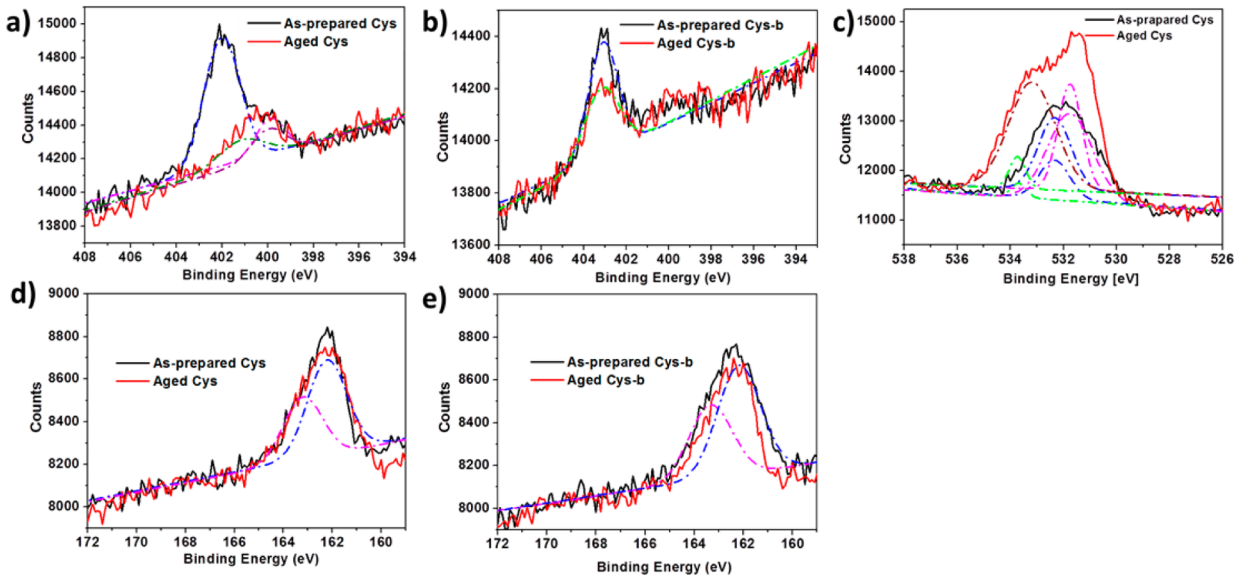

Figure 5. XPS spectrum of as-prepared Cys and Cys-b and those with the aging treatment. The (a, b) N 1s, (c) O 1s, and (d, e) S 2p spectra are included.

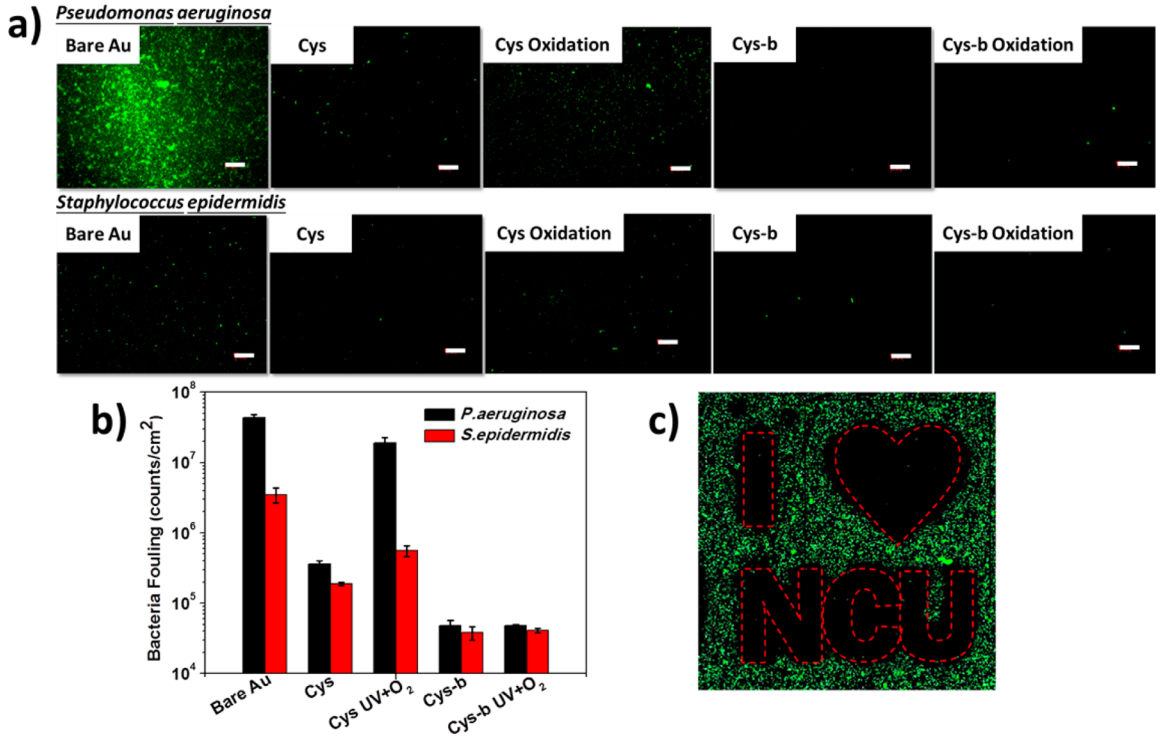

Figure 6. Bacterial adhesion tests on substrates of bare Au, Cys, Cys with aging, Cys-b, and Cys-b with aging. (a) Bacteria of *P. aeruginosa* and *S. epidermidis* were used in the tests and imaged using fluorescence microscopy. The scale bars in the images are 20 μm. (b) The quantitative results for bacterial adsorption on all substrates were estimated using ImageJ software. (c) The patterned feature of "I (heart) NCU" with Cys-b was prepared on the gold substrate. The image was taken after culturing with *P. aeruginosa* and washing with PBS. The red dashed lines were added as visual guides.

sulfur via the S 2p spectra. Herein, we found only bound sulfur, with the S $2p_{3/2}$ peak of the doublet at ~162 eV for all samples, which we assign as the thiolate group on a metal surface (Figure 5d, e).[41,55] The peak at 167.5 eV, associated with oxidized sulfur, is not observed in the two samples.[28] Thus, we confirmed that the aging of both types of SAMs (Cys and Cys-b) under air and light does not lead to the oxidation of the thiolate groups,[41,56] and also verified that the consequence of reduced wettability on the Cys SAMs should be ascribed to the conversion of $-NH_2$ to $-NO$.

Antifouling Properties of Cys-b SAMs. Cys and Cys-b SAMs were used for fouling resistance tests in the presence of bacteria, proteins, and mammalian cells. For the bacterial adhesion, the Gram-negative, *P. aruginosa*, and Gram-positive, *S. epidermidis*, bacteria were dissolved in PBS and incubated with substrates at 37 °C for 3 h, followed by washing with PBS

DOI: 10.1021/acsami.5b08418
ACS Appl. Mater. Interfaces 2015, 7, 23776−23786

and staining with fluorescence dye. As shown in the fluorescence images in Figure 6a, the green objects represent the adsorbed bacteria. Clearly, the surfaces modified with Cys and Cys-b can effectively reduce bacterial adsorption for both bacteria. However, after photooxidation, the numbers of bacteria on the Cys SAMs increased, while the Cys-b SAMs still exhibited antifouling capability. The quantitative data for bacterial adsorption are shown in Figure 6b, revealing that Cys-b can reduce the bacterial adhesion by 99.9% and 98.9% for *P. aeruginosa* and *S. epidermidis*, respectively, relative to that on bare gold surfaces. More strikingly, the gold substrate was patterned with Cys-b to generate a feature of "I (heart) NCU" as illustrated in Figure 6c. The majority of *P. aeruginosa* appear on the unmodified area as the manifesting image of the feature. Thus, the results presented here demonstrate the ability of the zwitterionic Cys-b coating to resist not only photooxidation, but also bacterial adsorption.

The nonspecific adsorption of proteins on medical devices can lead to adverse immune responses, thrombosis, infection, and reduced circulation time.[21] We utilized three proteins, mucin, lysozyme, and BSA, to evaluate the fouling resistance of the Cys and Cys-b SAMs. The adsorption levels were measured by performing ELISA (Figure 7). The results indicated that the

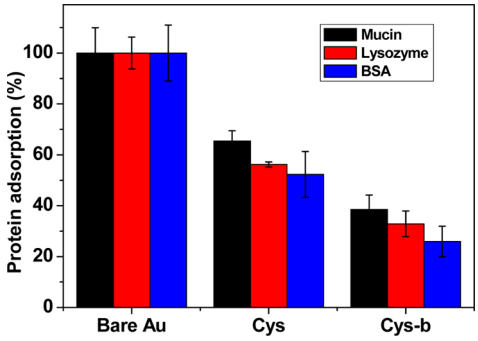

Figure 7. Protein adsorption with mucin, lysozyme, and BSA on bare Au, Cys, and Cys-b substrates. The relative adsorption levels were estimated by ELISA.

adsorption of proteins on Cys and Cys-b SAMs are in the order of mucin > lysozyme > BSA. The high adsorption levels of mucin might be due to the fact that it is a heavily glycosylated protein and is a key component in most gel-like secretions. Studies have shown that overexpressed exopolysaccharide molecules on bacteria can selectively interact with protein-resistant CB polymers, likely via hydrogen bonding.[57] The results presented here suggest that the Cys and Cys-b coatings with branched ionic structure exhibit similar behavior as CB materials.

Very recently, Jiang's group conducted systematic molecular simulation studies on the influence of charged groups on the antifouling properties of zwitterionic moieties.[23,58−60] The researchers found that the zwitterionic pair comprising quaternary ammonium and carboxylate exhibit the strongest capability to resist nonspecific adsorption among the 12 ionic combinations. This phenomenon can be attributed to strong hydration, low self-association of ionic groups, and low electrostatic attractions to proteins. In addition, the primary amine group tended to associate with the carboxylate group via hydrogen bonding, leading to a compromise in the hydrophilicity of the zwitterionic moiety. Their findings provide an important theoretical basis for our work. In the protein and bacteria fouling tests, Cys-b displayed stronger resistance than Cys, which is consistent with the simulation findings. Although the capability of Cys-b in protein repulsion is less effective than most polymer-based coatings, which can accomplish "ultra-low fouling",[61,62] it offers a great improvement over Cys and can be used when very thin (i.e., subnanometer) coatings are required.

In parallel studies, mammalian cells were brought into contact with surfaces to observe the cell adhesion and stretching dynamic equilibrium between the cell and the matrix, which are considered as crucial factors to cell physiology and manifested as the cellular number and spreading area.[63] NIH 3T3 fibroblasts were seeded on the bare Au, Cys, and Cys-b substrates to assess their resulting cell numbers and morphology. In Figure 8a, the 3T3 cells were observed microscopically after incubation for 3 days. The images indicate that the number of adhered cells on bare Au was greater than those on the SAM-modified substrates. In addition, the cells on bare Au adopt bipolar shapes, whereas those on the Cys and Cys-b SAMs were all round in appearance. The estimations for the corresponding 3T3 cells on the surfaces are presented in Figure 8b, which shows that the cells were less likely to adhere on the SAM-modified surfaces, particularly on the Cys-b SAM. In contrast, cells were able to anchor and spread on the bare Au surface. Because of fouling resistance of the Cys and Cys-b coatings, the adhesion and spreading of fibroblasts were considerably restrained, reflecting the poor amenability of these surfaces toward cell growth.

Modification of Hollow Ag@Au Nanoshells. The adsorbates Cys and Cys-b were employed as capping ligands for the modification of nanoparticles to enhance their biocompatibility and colloidal stability. We chose to examine the modification of hollow Ag@Au nanoshells due to their ease of synthesis and capacity to respond to near-infrared (NIR) light, which renders them useful in nanoparticle-based theranostics.[36,37] The hydrodynamic size and SPR band maxima of as-prepared nanoshells were examined using DLS and UV−vis spectroscopy and found to exhibit 146.3 ± 10.2 nm in diameter and 816 nm exctinction, respectively. After treatment with Cys and Cys-b, the extinction maxima underwent a red shift to 840 and 842 nm, respectively (Figure 9a). The shifts are due to the change in the refractive index at the interfaces arising from the self-assembly of the adsorbates on nanoshells, leading to changes in coupling of the incident light.

Figure 9b illustrates the effectiveness of the as-prepared and SAM-modified hollow Ag@Au nanoshells to induce heating in the surrounding medium. The nanoparticles were dissolved in PBS solution and irradiated at a wavelength of 808 nm with a power density of 4.6 W/cm^2. The temperature of the solution containing the nanoshells with and without surface engineering was measured at intervals of 10 s over a period of 10 min. During this time interval, the temperature of the bulk solution increased from 24 to ∼54 °C. In contrast, the temperature of the PBS solution in the absence of nanoshells only slightly increased with NIR irradiation from 24 to 28 °C, which is attributed to the absorption of heat from the laser. Therefore, the results demonstrate the capacity of these nanoshell structures for use in photothermal applications.

To investigate further their potential use in theranostics, we evaluated the long-term colloidal stability of modified hollow Ag@Au nanoshells upon exposure to UV irradiation and storage in the ambient environment for 4 weeks, followed by examining their extinction spectra (Figure 10). The spectra for

DOI: 10.1021/acsami.5b08418
ACS Appl. Mater. Interfaces 2015, 7, 23776−23786

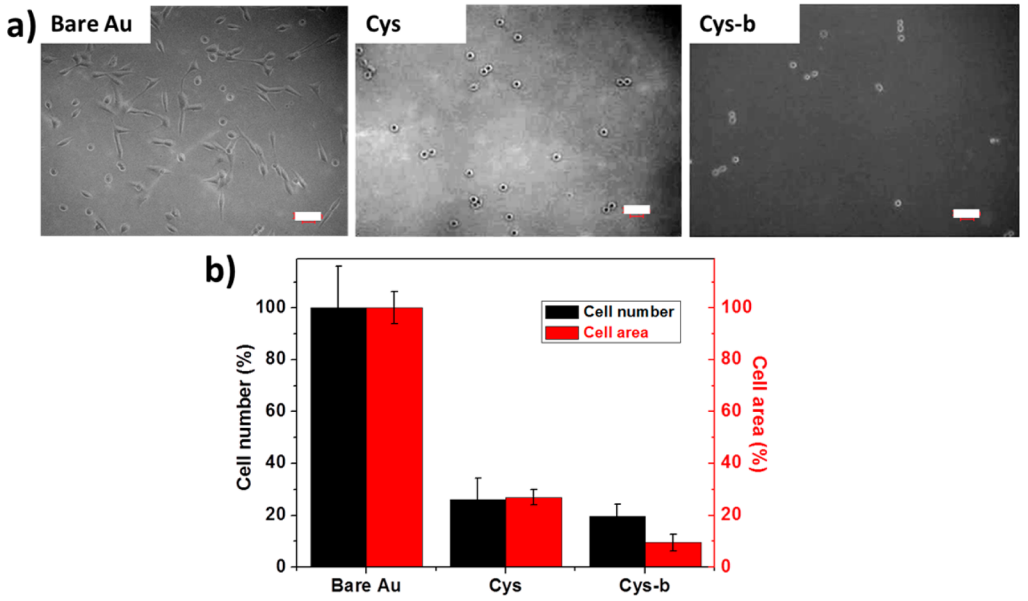

Figure 8. NIH 3T3 adhesion on bare Au, Cys, and Cys-b substrates. (a) Bright-field microscope images show the cell growth and spreading on bare Au, Cys, and Cys-b substrates. The scale bars are 200 μm. (b) Relative cell adsorbed number and cell spreading area were estimated using ImageJ software.

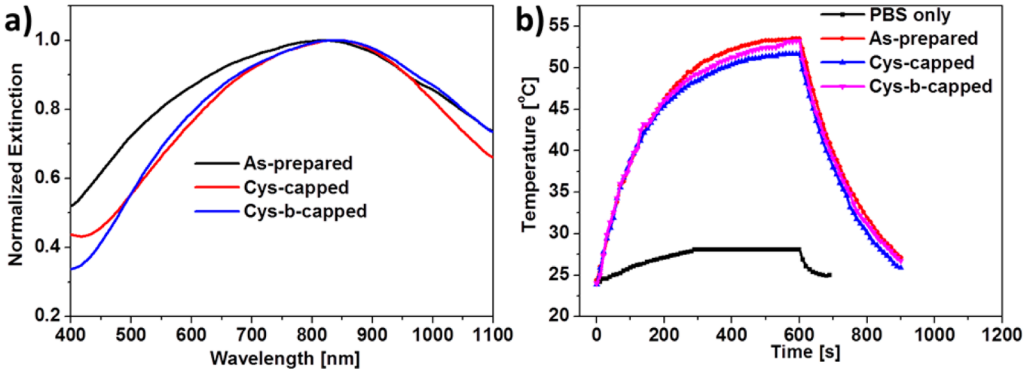

Figure 9. (a) Extinction spectra of the as-prepared, Cys- and Cys-*b*-capped hollow Ag@Au nanoshells. (b) Temperature of the PBS solutions containing hollow Ag@Au nanoshells upon exposure to laser irradiation at 808 nm. Measurements were collected at 30 s intervals over 10 min and compared to the response of pure PBS (with no nanoshells added).

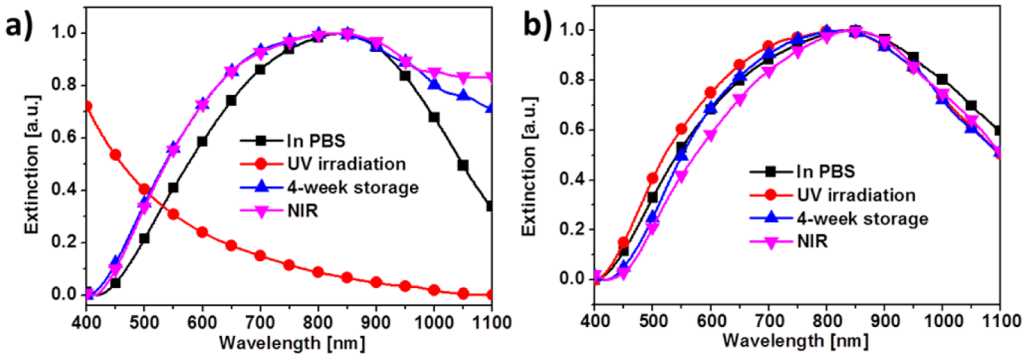

Figure 10. Long-term colloidal stability of hollow Ag@Au nanoshells with modification of (a) Cys and (b) Cys-b, monitored by using UV−vis spectroscopy. The stability of the nanoshells were evaluated by exposure to UV irradiation, storage in the ambient environment for 4 weeks and NIR irradiation, followed by examining using UV−vis spectroscopy.

the nanoshells capped with Cys and Cys-b are shown in Figure 10a and 10b, respectively. After UV irradiation for 12 h at rt, the extinction band of the nanoshells with Cys modification disappeared, whereas the sample with Cys-b modification remained strong, with a peak maxima at 824 nm. The results reflect the better photostability of nanoparticles decorated with Cys-b compared to Cys, most likely due to the exclusive photoinduced oxidation of Cys, as we observed on planar Au

DOI: 10.1021/acsami.5b08418
ACS Appl. Mater. Interfaces 2015, 7, 23776−23786

surfaces and reported above. In addition, after storage for four weeks, the extinction spectrum of the Cys-capped nanoshells exhibited broadening, indicating a decrease in particle size in accordance with quantum size theories.[64,65] In contrast, the Cys-*b*-capped nanoshells showed good colloidal stability throughout the storage time. Herein, after the short-term exposure (10 min) to NIR, nanoshells modified with both Cys and Cys-b retained their colloidal stability, which reflects the comparable photothermal properties.

The chemical and colloidal stability of metal nanoparticles under various conditions has become increasingly important for their wide spectrum of applications. In this work, we examined the susceptibility of Cys-b nanoshells to Cu^{2+} by using UV−vis spectroscopy and visual inspection. As shown in Figure 11, after

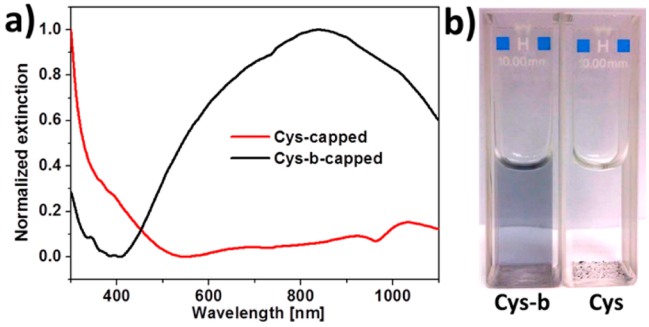

Figure 11. (a) Extinction spectrum and (b) visual inspection of Cys- and Cys-*b*-capped nanoshells in the presence of Cu^{2+}. A 1 mM Cu^{2+} solution in deionized water was prepared for the interaction with modified nanoshells at rt for 1 h.

1 h incubation at rt, the spectra and photograph of the Cys-capped nanoshells showed aggregation and sedimentation of particles in agreement with previous studies.[32,33] In contrast, the Cys-*b*-modified nanoshells remained dispersed in the aqueous solution. The absence of the interaction of Cys-b with Cu^{2+}can be attributed to the lack of donating electrons from the lone electron pair into an empty metal orbital. Therefore, these results confirmed that the bioinspired Cys-b capping ligand displays the tolerance to Cu^{2+} and affords a wider spectrum of applications under complex conditions.

CONCLUSIONS

We developed the bioinspired zwitterionic surface ligand Cys-b with robust antifouling, antiphotooxidation, and environmentally benign properties for nanoscale coatings applications and colloidal modification. The amphoteric Cys-b was synthesized by quaternization of the amino group of Cys, facilitating a durable zwitterionic form over a wide pH range (3.4 to 10.8). The occupation of all free electrons of the amine group in Cys-b by the quaternization prevents photoinduced oxidization on gold surfaces as demonstrated by contact angle measurements, XPS, and bacterial adsorption studies. In addition, Cys-b exhibits enhanced fouling resistance against bacteria, proteins, and cells, which is most likely due to its strong hydration, low self-association of ionic groups, and low electrostatic attraction to proteins. Additional practical implementations of Cys-b were demonstrated via the modification of plasmonic hollow Ag@Au nanoshells, showing excellent colloidal stability and avoiding aggregation/precipitation in the presence of Cu^{2+}. As such, Cys-b holds great promise as a surface-modifying agent on flat (2D) surfaces and on nanoparticles. Our work also provides molecular level insight into the development of zwitterionic coating materials that resist photoinduced oxidation and coordination with Cu^{2+}.

ASSOCIATED CONTENT

Supporting Information

The Supporting Information is available free of charge on the ACS Publications website at DOI: 10.1021/acsami.5b08418.

Synthesis procedure of Cys-b and 1H NMR spectrum of Cys-b, Figure S1; contact angle measurements for Cys- and Cys-*b*-modified substrates, Figure S2; atomic concentrations from XPS measurements, Table S1 (PDF)

AUTHOR INFORMATION

Corresponding Author

*E-mail: cjhuang@ncu.edu.tw.

Notes

The authors declare no competing financial interest.

ACKNOWLEDGMENTS

The authors acknowledge the Ministry of Science and Technology (MOST 104-2221-E-008-108) for financial support of this project. Research efforts at the University of Houston were generously supported by the National Science Foundation (CHE-1411265), the Robert A. Welch Foundation (E-1320), and the Texas Center for Superconductivity at the University of Houston.

REFERENCES

(1) Jain, R. K.; Stylianopoulos, T. Delivering Nanomedicine to Solid Tumors. *Nat. Rev. Clin. Oncol.* **2010**, *7* (11), 653−664.

(2) Sao, R.; Vaish, R.; Sinha, N. Multifunctional Drug Delivery Systems Using Inorganic Nanomaterials: A Review. *J. Nanosci. Nanotechnol.* **2015**, *15* (3), 1960−1972.

(3) Wicki, A.; Witzigmann, D.; Balasubramanian, V.; Huwyler, J. Nanomedicine in Cancer Therapy: Challenges, Opportunities, and Clinical Applications. *J. Controlled Release* **2015**, *200*, 138−157.

(4) Howes, P. D.; Chandrawati, R.; Stevens, M. M. Colloidal Nanoparticles as Advanced Biological Sensors. *Science* **2014**, *346* (6205), 1247390.

(5) Raynor, J. E.; Capadona, J. R.; Collard, D. M.; Petrie, T. A.; Garcia, A. J. Polymer Brushes and Self-Assembled Monolayers: Versatile Platforms to Control Cell Adhesion to Biomaterials (Review). *Biointerphases* **2009**, *4* (2), FA3−FA16.

(6) Katti, D. S.; Shanmugam, K.; Vasita, R. Improved Biomaterials for Tissue Engineering Applications: Surface Modification of Polymers. *Curr. Top. Med. Chem.* **2008**, *8* (4), 341−353.

(7) Chen, S. F.; Li, L. Y.; Zhao, C.; Zheng, J. Surface Hydration: Principles and Applications Toward Low-Fouling/Nonfouling Biomaterials. *Polymer* **2010**, *51* (23), 5283−5293.

(8) Love, J. C.; Estroff, L. A.; Kriebel, J. K.; Nuzzo, R. G.; Whitesides, G. M. Self-Assembled Monolayers of Thiolates on Metals as a Form of Nanotechnology. *Chem. Rev.* **2005**, *105* (4), 1103−1169.

(9) Nuzzo, R. G.; Dubois, L. H.; Allara, D. L. Fundamental-Studies of Microscopic Wetting on Organic-Surfaces. 1. Formation and Structural Characterization of a Self-Consistent Series of Polyfunctional Organic Monolayers. *J. Am. Chem. Soc.* **1990**, *112* (2), 558−569.

(10) Kondoh, H.; Kodama, C.; Nozoye, H. Structure-Dependent Change of Desorption Species from n-Alkanethiol Monolayers Adsorbed on Au(111): Desorption of Thiolate Radicals from Low-Density Structures. *J. Phys. Chem. B* **1998**, *102* (13), 2310−2312.

(11) Roberts, M. J.; Bentley, M. D.; Harris, J. M. Chemistry for Peptide and Protein PEGylation. *Adv. Drug Delivery Rev.* **2002**, *54* (4), 459−476.

DOI: 10.1021/acsami.5b08418
ACS Appl. Mater. Interfaces 2015, 7, 23776−23786

(12) Moghimi, S. M.; Hunter, A. C.; Murray, J. C. Long-Circulating and Target-Specific Nanoparticles: Theory to Practice. *Pharmacol. Rev.* **2001**, *53* (2), 283−318.
(13) Wang, J. Q.; Sui, M. H.; Fan, W. M. Nanoparticles for Tumor Targeted Therapies and Their Pharmacokinetics. *Curr. Drug Metab.* **2010**, *11* (2), 129−141.
(14) Han, S.; Kim, C.; Kwon, D. Thermal-Degradation of Poly(Ethylene Glycol). *Polym. Degrad. Stab.* **1995**, *47* (2), 203−208.
(15) Han, S.; Kim, C.; Kwon, D. Thermal/Oxidative Degradation and Stabilization of Polyethylene Glycol. *Polymer* **1997**, *38* (2), 317−323.
(16) Li, L. Y.; Chen, S. F.; Jiang, S. Y. Protein Interactions with Oligo(Ethylene Glycol) (OEG) Self-Assembled Monolayers: OEG Stability, Surface Packing Density and Protein Adsorption. *J. Biomater. Sci., Polym. Ed.* **2007**, *18* (11), 1415−1427.
(17) Choi, H. S.; Liu, W.; Misra, P.; Tanaka, E.; Zimmer, J. P.; Ipe, B. I.; Bawendi, M. G.; Frangioni, J. V. Renal Clearance of Quantum Dots. *Nat. Biotechnol.* **2007**, *25* (10), 1165−1170.
(18) Estephan, Z. G.; Schlenoff, P. S.; Schlenoff, J. B. Zwitteration As an Alternative to PEGylation. *Langmuir* **2011**, *27* (11), 6794−6800.
(19) Schlenoff, J. B. Zwitteration: Coating Surfaces with Zwitterionic Functionality to Reduce Nonspecific Adsorption. *Langmuir* **2014**, *30* (32), 9625−9636.
(20) Holmlin, R. E.; Chen, X. X.; Chapman, R. G.; Takayama, S.; Whitesides, G. M. Zwitterionic SAMs That Resist Nonspecific Adsorption of Protein from Aqueous Buffer. *Langmuir* **2001**, *17* (9), 2841−2850.
(21) Jiang, S. Y.; Cao, Z. Q. Ultralow-Fouling, Functionalizable, and Hydrolyzable Zwitterionic Materials and Their Derivatives for Biological Applications. *Adv. Mater.* **2010**, *22* (9), 920−932.
(22) Huang, C. J.; Brault, N. D.; Li, Y. T.; Yu, Q. M.; Jiang, S. Y. Controlled Hierarchical Architecture in Surface-Initiated Zwitterionic Polymer Brushes with Structurally Regulated Functionalities. *Adv. Mater.* **2012**, *24* (14), 1834−1837.
(23) Shao, Q.; Jiang, S. Y. Molecular Understanding and Design of Zwitterionic Materials. *Adv. Mater.* **2015**, *27* (1), 15−26.
(24) Liu, W. H.; Choi, H. S.; Zimmer, J. P.; Tanaka, E.; Frangioni, J. V.; Bawendi, M. Compact Cysteine-Coated CdSe(ZnCdS) Quantum Dots for In Vivo Applications. *J. Am. Chem. Soc.* **2007**, *129* (47), 14530−14531.
(25) Breus, V. V.; Heyes, C. D.; Tron, K.; Nienhaus, G. U. Zwitterionic Biocompatible Quantum Dots for Wide pH Stability and Weak Nonspecific Binding to Cells. *ACS Nano* **2009**, *3* (9), 2573−2580.
(26) Jiang, X. E.; Rocker, C.; Hafner, M.; Brandholt, S.; Dorlich, R. M.; Nienhaus, G. U. Endo- and Exocytosis of Zwitterionic Quantum Dot Nanoparticles by Live HeLa Cells. *ACS Nano* **2010**, *4* (11), 6787−6797.
(27) Rosen, J. E.; Gu, F. X. Surface Functionalization of Silica Nanoparticles with Cysteine: A Low-Fouling Zwitterionic Surface. *Langmuir* **2011**, *27* (17), 10507−10513.
(28) Lee, S. H.; Lin, W. C.; Kuo, C. H.; Karakachian, M.; Lin, Y. C.; Yu, B. Y.; Shyue, J. J. Photooxidation of Amine-Terminated Self-Assembled Monolayers on Gold. *J. Phys. Chem. C* **2010**, *114* (23), 10512−10519.
(29) Huang, C. J.; Wang, L. C.; Liu, C. Y.; Chiang, A. S. T.; Chang, Y. C. Natural Zwitterionic Organosulfurs as Surface Ligands for Antifouling and Responsive Properties. *Biointerphases* **2014**, *9* (2), 029010.
(30) Zakaria, H. M.; Shah, A.; Konieczny, M.; Hoffmann, J. A.; Nijdam, A. J.; Reeves, M. E. Small Molecule- and Amino Acid-Induced Aggregation of Gold Nanoparticles. *Langmuir* **2013**, *29* (25), 7661−7673.
(31) Liu, J. M.; Wang, H. F.; Yan, X. P. A Gold Nanorod Based Colorimetric Probe for the Rapid and Selective Detection of Cu2+ Ions. *Analyst* **2011**, *136* (19), 3904−3910.
(32) Foroushani, A.; Zhang, Y. C.; Li, D.; Mathesh, M.; Wang, H. B.; Yan, F. H.; Barrow, C. J.; He, J.; Yang, W. R. Tunnelling Current Recognition Through Core-Satellite Gold Nanoparticles for Ultra-sensitive Detection of Copper Ions. *Chem. Commun.* **2015**, *51* (14), 2921−2924.
(33) Ndokoye, P.; Ke, J.; Liu, J.; Zhao, Q. D.; Li, X. Y. L-Cysteine-Modified Gold Nanostars for SERS-Based Copper Ions Detection in Aqueous Media. *Langmuir* **2014**, *30* (44), 13491−13497.
(34) Wang, H.; Chen, S.; Li, L.; Jiang, S. Improved Method for the Preparation of Carboxylic Acid and Amine Terminated Self-Assembled Monolayers of Alkanethiolates. *Langmuir* **2005**, *21* (7), 2633−2636.
(35) Lee, P. C.; Meisel, D. Adsorption and Surface-Enhanced Raman of Dyes on Silver and Gold Sols. *J. Phys. Chem.* **1982**, *86*, 3391−3395.
(36) Vongsayat, V.; Vittur, B. M.; Bryan, W. W.; Kim, J. H.; Lee, T. R. Ultrasmall Hollow Gold-Silver Nanoshells with Extinctions Strongly Red-Shifted to the Near-Infrared. *ACS Appl. Mater. Interfaces* **2011**, *3* (9), 3616−3624.
(37) Li, C. H.; Jamison, A. C.; Rittikulsittichai, S.; Lee, T. C.; Lee, T. R. In Situ Growth of Hollow Gold-Silver Nanoshells within Porous Silica Offers Tunable Plasmonic Extinctions and Enhanced Colloidal Stability. *ACS Appl. Mater. Interfaces* **2014**, *6* (22), 19943−19950.
(38) Oldenburg, S. J.; Averitt, R. D.; Westcott, S. L.; Halas, N. J. Nanoengineering of Optical Resonances. *Chem. Phys. Lett.* **1998**, *288* (2−4), 243−247.
(39) Schubert, M. P. Combination of Thiol Acids with Methylglyoxal. *J. Biol. Chem.* **1935**, *111*, 671−678.
(40) Grafius, M. A.; Neilands, J. B. Apparent Dissociation Constants of Cysteine Derivatives. *J. Am. Chem. Soc.* **1955**, *77* (12), 3389−3390.
(41) Wang, H.; Chen, S. F.; Li, L. Y.; Jiang, S. Y. Improved Method for the Preparation of Carboxylic Acid and Amine Terminated Self-Assembled Monolayers of Alkanethiolates. *Langmuir* **2005**, *21* (7), 2633−2636.
(42) Shin, T.; Kim, K. N.; Lee, C. W.; Shin, S. K.; Kang, H. Self-Assembled Monolayer of L-Cysteine on Au(111): Hydrogen Exchange Between Zwitterionic L-Cysteine and Physisorbed Water. *J. Phys. Chem. B* **2003**, *107* (42), 11674−11681.
(43) Uvdal, K.; Bodo, P.; Liedberg, B. L-Cysteine Adsorbed on Gold and Copper-An X-Ray Photoelectron-Spectroscopy Study. *J. Colloid Interface Sci.* **1992**, *149* (1), 162−173.
(44) Cavalleri, O.; Gonella, G.; Terreni, S.; Vignolo, M.; Floreano, L.; Morgante, A.; Canepa, M.; Rolandi, R. High Resolution X-Ray Photoelectron Spectroscopy of L-Cysteine Self-Assembled Films. *Phys. Chem. Chem. Phys.* **2004**, *6* (15), 4042−4046.
(45) Huang, C. J.; Wang, L. C.; Shyue, J. J.; Chang, Y. C. Developing Antifouling Biointerfaces Based on Bioinspired Zwitterionic Dopamine through pH-Modulated Assembly. *Langmuir* **2014**, *30* (42), 12638−12646.
(46) Shen, C. H.; Cho, Y. J.; Lin, Y. C.; Chien, L. C.; Lee, T. M.; Chuang, W. H.; Lin, J. C., Surface Modification of Titanium Substrate with a Novel Covalently-Bound Copolymer Thin Film for Improving Its Platelet Compatibility. *J. Mater. Sci.: Mater. Med.* **2015**, *26* (2), 10.1007/s10856-015-5420-8.
(47) Yeh, S. B.; Chen, C. S.; Chen, W. Y.; Huang, C. J. Modification of Silicone Elastomer with Zwitterionic Silane for Durable Antifouling Properties. *Langmuir* **2014**, *30* (38), 11386−11393.
(48) Yang, R.; Gleason, K. K. Ultrathin Antifouling Coatings with Stable Surface Zwitterionic Functionality by Initiated Chemical Vapor Deposition (iCVD). *Langmuir* **2012**, *28* (33), 12266−12274.
(49) Schoenfisch, M. H.; Pemberton, J. E. Air Stability of Alkanethiol Self-Assembled Monolayers on Silver and Gold Surfaces. *J. Am. Chem. Soc.* **1998**, *120* (18), 4502−4513.
(50) Chinwangso, P.; Jamison, A. C.; Lee, T. R. Multidentate Adsorbates for Self-Assembled Monolayer Films. *Acc. Chem. Res.* **2011**, *44* (7), 511−519.
(51) Singhana, B.; Jamison, A. C.; Hoang, J.; Lee, T. R. Self-Assembled Monolayer Films Derived from Tridentate Cyclohexyl Adsorbates with Alkyl Tailgroups of Increasing Chain Length. *Langmuir* **2013**, *29* (46), 14108−14116.
(52) Srisombat, L. O.; Zhang, S. S.; Lee, T. R. Thermal Stability of Mono-, Bis-, and Tris-Chelating Alkanethiol Films Assembled on Gold Nanoparticles and Evaporated "Flat" Gold. *Langmuir* **2010**, *26* (1), 41−46.

DOI: 10.1021/acsami.5b08418
ACS Appl. Mater. Interfaces 2015, 7, 23776−23786

(53) Iqbal, M. Z.; Katsiotis, M. S.; Alhassan, S. M.; Liberatore, M. W.; Abdala, A. A. Effect of Solvent on the Uncatalyzed Synthesis of Aminosilane-Functionalized Graphene. *RSC Adv.* **2014**, *4* (13), 6830−6839.
(54) Batich, C. D.; Donald, D. S. X-Ray Photoelectron Spectroscopy of Nitroso Componds: Relative Ionicity of the Closed and Open Forms. *J. Am. Chem. Soc.* **1984**, *106* (10), 2758−2761.
(55) Laibinis, P. E.; Whitesides, G. M.; Allara, D. L.; Tao, Y. T.; Parikh, A. N.; Nuzzo, R. G. Comparison of the Structures and Wetting Properties of Self-Assembled Monolayers of Normal-Alkanethiols on the Coinage Metal Surfaces, Cu, Ag, Au. *J. Am. Chem. Soc.* **1991**, *113* (19), 7152−7167.
(56) Techane, S. D.; Gamble, L. J.; Castner, D. G. Multitechnique Characterization of Self-Assembled Carboxylic Acid-Terminated Alkanethiol Monolayers on Nanoparticle and Flat Gold Surfaces. *J. Phys. Chem. C* **2011**, *115* (19), 9432−9441.
(57) Huang, C. J.; Mi, L.; Jiang, S. Y. Interactions of Alginate-Producing and -Deficient Pseudomonas Aeruginosa with Zwitterionic Polymers. *Biomaterials* **2012**, *33* (14), 3626−3631.
(58) Shao, Q.; Jiang, S. Y. Influence of Charged Groups on the Properties of Zwitterionic Moieties: A Molecular Simulation Study. *J. Phys. Chem. B* **2014**, *118* (27), 7630−7637.
(59) Shao, Q.; Mi, L.; Han, X.; Bai, T.; Liu, S. J.; Li, Y. T.; Jiang, S. Y. Differences in Cationic and Anionic Charge Densities Dictate Zwitterionic Associations and Stimuli Responses. *J. Phys. Chem. B* **2014**, *118* (24), 6956−6962.
(60) Shao, Q.; White, A. D.; Jiang, S. Y. Difference of Carboxybetaine and Oligo(ethylene glycol) Moieties in Altering Hydrophobic Interactions: A Molecular Simulation Study. *J. Phys. Chem. B* **2014**, *118* (1), 189−194.
(61) Huang, C. J.; Li, Y. T.; Krause, J. B.; Brault, N. D.; Jiang, S. Y. Internal Architecture of Zwitterionic Polymer Brushes Regulates Nonfouling Properties. *Macromol. Rapid Commun.* **2012**, *33* (11), 1003−1007.
(62) Chen, S. F.; Jiang, S. Y. A New Avenue to Nonfouling Materials. *Adv. Mater.* **2008**, *20* (2), 335.
(63) Cukierman, E.; Pankov, R.; Yamada, K. M. Cell Interactions with Three-Dimensional Matrices. *Curr. Opin. Cell Biol.* **2002**, *14* (5), 633−639.
(64) Addison, C. J.; Brolo, A. G. Nanoparticle-Containing Structures as a Substrate for Surface-Enhanced Raman Scattering. *Langmuir* **2006**, *22* (21), 8696−8702.
(65) Meyer, M.; Le Ru, E. C.; Etchegoin, P. G. Self-Limiting Aggregation Leads to Long-Lived Metastable Clusters in Colloidal Solutions. *J. Phys. Chem. B* **2006**, *110* (12), 6040−6047.

DOI: 10.1021/acsami.5b08418
ACS Appl. Mater. Interfaces 2015, 7, 23776−23786